SIAM J. APPL. MATH.
Vol. 70, No. 7, pp. 2373–2389

TRAVELING WAVES IN DEEP WATER WITH GRAVITY AND SURFACE TENSION*

BENJAMIN AKERS† AND DAVID P. NICHOLLS†

Abstract. This paper is concerned with the simulation of periodic traveling deep-water free-surface water waves under the influence of gravity and surface tension in two and three dimensions. A variety of techniques is utilized, including the numerical simulation of a weakly nonlinear model, explicit solutions of low-order perturbation theories, and the direct numerical simulation of the full water wave equations. The weakly nonlinear models which we present are new and extend the work of Akers and Milewski [*SIAM J. Appl. Math.*, 70 (2010), pp. 2390–2408] to arbitrary Bond number and fluid depth. The numerical scheme for the full water wave problem features a novel extension of the "Transformed Field Expansions" method of Nicholls and Reitich [*Euro. J. Mech. B Fluids*, 25 (2006), pp. 406–424] to accommodate capillary effects in a stable and rapid fashion. The purpose of this paper is apply the new numerical method, then compare small amplitude solutions of potential flow with those of the approximate model. Particular attention is paid to the behavior near quadratic resonances, an example of which is the *Wilton ripple*.

Key words. potential flow, surface tension, ripples

AMS subject classifications. 74J30, 76B15, 76B45, 76B07

DOI. 10.1137/090771351

1. Introduction. Traveling water waves have been studied for over a century, most famously by Stokes, for whom weakly nonlinear periodic waves are now named [1, 2]. In his 1847 paper, Stokes expanded the wave profile as a power series in a small wave slope parameter, a technique which has since become commonplace. This classic perturbation expansion, which we will refer to as the Stokes expansion, has since been applied to the water wave problem numerous times [3, 4, 5, 6, 7, 8]. When the effect of surface tension is included, an expansion in wave amplitude may be singular due to a resonance between a long and a short wave, as noted first in [9] and more recently in [10, 11, 12, 13]. In this paper, we use both numerical solutions and asymptotic predictions from a Stokes expansion to compare periodic traveling solutions of the potential flow equations, as in [14], to those in a weakly nonlinear model extending [15]. The goal is to compare solutions of the potential flow equations to those of a quadratic nonlinear model, in the neighborhood of resonances which occur at quadratic order in a perturbation series expansion. Near these resonances, perturbation series expansions about a Stokes wave will not be valid; the quadratic model may provide a better approximation.

Traveling waves on both a two-dimensional (one horizontal and one vertical dimension) and a three-dimensional fluid will be computed. The three-dimensional waves we examine are periodic in both horizontal space dimensions, commonly referred to as short-crested waves [16]. Short-crested wave solutions to the potential flow equations have been computed previously without surface tension [14, 17, 18] and with surface tension [19]. They have also been studied experimentally [20, 21]. A significant contribution of the current work is the presentation of a new numeri-

*Received by the editors September 16, 2009; accepted for publication (in revised form) March 22, 2010; published electronically June 9, 2010.
http://www.siam.org/journals/siap/70-7/77135.html
†Department of Mathematics, Statistics, and Computer Science, University of Illinois at Chicago, 851 S. Morgan, Chicago, IL 60607 (akers@math.uic.edu, nicholls@math.uic.edu). The work of the second author was supported by the NSF through grant DMS-0810958.

cal method for computing such solutions to the potential flow equations. The new numerical method is an extension of that in [14] to compute traveling waves with surface tension; the previous algorithm did not include capillary forces. In addition, we compare small amplitude solutions in the potential flow equations to those in a weakly nonlinear model, specifically by their speed-amplitude curves. We choose the speed-amplitude curves as a basis for comparison because of the relationship between the waves' stability and their speed-amplitude dependence. In many water waves models, families of waves may change stability only at extrema of their speed-energy curve [22, 23, 24]. In addition, the sign of the speed correction, referred to later as c_2, of a weakly nonlinear wave is predictive with respect to dynamics of wave packets, due to the role that this correction plays as a coefficient in the nonlinear Schrödinger equation [25].

There is a long history of numerical implementation of the Stokes expansion to simulate water waves [26], with the approaches of [27, 28] and [14] of greatest relevance in the present context. However, only the latter of these two approaches can be *rigorously* shown to converge (proof in [29]; see Figure 1 in [14] for an explicit demonstration of the ill-conditioning present in the algorithm of [27]) and thus be completely reliable for numerical simulation. In this paper we make the nontrivial extension of this *Transformed Field Expansions* approach to include effects of surface tension.

The implicit assumption of the Stokes expansion that solutions are analytic in the wave height/slope parameter ϵ can also be exploited to derive weakly nonlinear model equations. In the case of shallow-water waves with surface tension, well-known weakly nonlinear models include the fifth-order Korteweg–de Vries (KdV) equation [30] and the Kadomtsev–Petviashvili (KP) equation [31]. Without surface tension Boussinesq-type models have been used to study weakly nonlinear short-crested waves, for example, in [32]. Recently analogues of both the fifth-order KdV [33] and KP equations [34] have been derived for deep-water gravity-capillary waves. In this paper we examine solutions to an *isotropic* weakly nonlinear model for deep-water gravity-capillary waves, an extension of the model derived in [15]. The numerical solutions to the weakly nonlinear model are compared to solutions of the potential flow equations via their speed-amplitude curves. Waves are computed on both a two-dimensional and a three-dimensional fluid. In both cases the numerical solutions are compared to asymptotic predictions. The validity of the weakly nonlinear truncation is explored, with special attention paid to behavior near resonances (the Wilton ripples).

The paper is organized as follows. In section 2, the model equations are presented, including a summary of the derivation of the weakly nonlinear model. In section 3, the numerical methods used for computing traveling waves are presented, including some sample simulations for each model. In section 4, the numerical results in each model equation are compared with the asymptotic predictions via the speed-amplitude plots. Conclusions and areas of future research are presented in section 5.

2. Model equations. To begin, we consider the potential flow equations for an incompressible fluid undergoing an irrotational flow [5]. For water ($\rho = 1\frac{\text{gm}}{\text{cm}^3}$) these equations take the dimensional form

$$\Delta\phi + \phi_{zz} = 0, \qquad -H_0 < z < \eta, \tag{2.1a}$$

$$\phi_z = 0, \qquad z = -H_0, \tag{2.1b}$$

$$\eta_t + \nabla\eta \cdot \nabla\phi = \phi_z, \qquad z = \eta, \tag{2.1c}$$

$$\text{(2.1d)}\quad \phi_t + \frac{1}{2}|\nabla\phi|^2 + \frac{1}{2}(\phi_z)^2 + g\eta - \gamma\nabla\cdot\left(\frac{\nabla\eta}{(1+|\nabla\eta|^2)^{1/2}}\right) = 0, \qquad z = \eta.$$

Here $\eta(x,y,t)$ is the free-surface displacement, $\phi(x,y,z,t)$ is the velocity potential, g is the gravitational constant, γ is the surface tension coefficient ($\gamma = 73.5\frac{\text{cm}^3}{\text{sec}^2}$ for an air-water interface), and H_0 is the undisturbed fluid depth [35]. Choosing a characteristic lengthscale L, surface displacement a, potential scale $P = a\sqrt{gL}$, timescale $T = L^{1/2}g^{-1/2}$, and nondimensionalizing yields

$$\text{(2.2a)}\qquad \Delta\phi + \phi_{zz} = 0, \qquad -H_1 < z < \epsilon\eta,$$

$$\text{(2.2b)}\qquad \phi_z = 0, \qquad z = -H_1,$$

$$\text{(2.2c)}\qquad \eta_t + \epsilon\nabla\eta\cdot\nabla\phi = \phi_z, \qquad z = \epsilon\eta,$$

$$\text{(2.2d)}\quad \phi_t + \frac{\epsilon}{2}\left(|\nabla\phi|^2 + (\phi_z)^2\right) + \eta - \frac{\sigma}{\epsilon}\nabla\cdot\left(\frac{\nabla\eta}{(1+|\nabla\eta|^2)^{1/2}}\right) = 0, \qquad z = \epsilon\eta.$$

In this model $\epsilon = a/L$ is the wave slope, and $H_1 = H_0/L$ measures the fluid depth relative to the period of the wave. The parameter $\sigma = \frac{\gamma}{gL^2}$, a Bond number, compares the force due to surface tension to that of gravity. Waves with $\sigma < 1$ are called gravity waves, those with $\sigma > 1$ are called capillary waves, and waves near $\sigma = 1$ are the hybrid, capillary-gravity waves. Often the Bond number is written in terms of the characteristic depth, $\frac{\gamma}{gH_0^2}$; however, this definition of the Bond number makes sense only when the depth is smaller than, or on the order of, the wavelength. Such a depth-based Bond number is zero for all wavelengths in deep water. The Bond number is meant to compare the relative importance of surface tension to gravity, but for deep-water waves ($H_1 \to \infty$), as will be studied here, using a depth-based Bond number leads to the conclusion that surface tension is negligible. As surface tension clearly dominates the dynamics of sufficiently short waves (even when $H_1 \to \infty$) one must use a horizontal lengthscale for the Bond number in deep water.

In this paper we investigate periodic traveling waves in not only the potential flow equations (2.2), but also a weakly nonlinear model which we derive below (we note that the case $\sigma = 1$ in deep water appears in [15]). To summarize the derivation for *arbitrary* σ and finite depth, we expand the free-surface boundary conditions (2.2c) and (2.2d) about the mean level $z = 0$. Taking the deep-water limit $H_1 \to \infty$ and solving Laplace's equation in the lower half-space eliminates the z-dependence of (2.2),

$$\phi(x,y,t,z) = \mathcal{F}^{-1}\left\{\mathcal{F}\left\{\Phi(x,y,t)\right\}e^{|\mathbf{k}|\mathbf{z}}\right\}.$$

Here $\mathcal{F}$ is the Fourier transform in (x,y) with dual variable $\mathbf{k}$; clearly $\Phi = \phi(x,y,t,0)$. Derivatives of ϕ with respect to z at $z = 0$ correspond to multiplication of the Fourier transform of Φ by $|\mathbf{k}|$, denoted by $(-\Delta)^{1/2}$ in physical space. This procedure simplifies the potential flow equations (2.2) to a system of two equations acting at the mean level $z = 0$. The new system, keeping terms to cubic order, is

$$\text{(2.3a)}\quad \eta_t - (-\Delta)^{1/2}\Phi + \epsilon\nabla\cdot(\eta\nabla\Phi) + \frac{\epsilon^2}{2}\nabla\cdot(\eta^2\nabla(-\Delta)^{1/2}\Phi) = 0,$$

$$\Phi_t + (1-\sigma\Delta)\eta + \epsilon\left(\frac{1}{2}(\nabla\Phi)^2 + \frac{1}{2}((-\Delta)^{1/2}\Phi)^2 + \eta(-\Delta)^{1/2}\Phi_t\right)$$

$$\text{(2.3b)}\quad + \frac{\epsilon^2}{2}\left(\sigma\nabla\cdot(\nabla\eta)^3 + 2\eta(\nabla\Phi\cdot\nabla(-\Delta)^{1/2}\Phi - \Delta\Phi(-\Delta)^{1/2}\Phi) - \eta^2\Delta\Phi_t\right) = 0.$$

The system (2.3) can be formally rewritten in terms of only Φ or η. Eliminating Φ in favor of η and truncating at quadratic order yields

$$\eta_{tt} + \Omega^2 \eta + \epsilon N(\eta, \eta_t) = 0, \tag{2.4}$$

with

$$N(\eta, \eta_t) = (-\Delta)^{1/2} \left(\frac{1}{2} (\mathcal{H}\eta_t)^2 + \frac{1}{2}\eta_t^2 - \eta \Omega^2 \eta \right) - \nabla \cdot (\eta S \nabla \eta + \eta_t \mathcal{H} \eta_t)$$

and

$$S = (1 - \sigma\Delta), \qquad \Omega^2 = (1 - \sigma\Delta)(-\Delta)^{1/2}, \qquad \mathcal{H} = -\nabla(-\Delta)^{-1/2}.$$

The operator $\mathcal{H}$ is the Hilbert transform with Fourier symbol $\hat{\mathcal{H}} = -i\frac{\mathbf{k}}{|\mathbf{k}|}$. Similar techniques can be used to write quadratic truncations in terms of Φ [39]. Equation (2.4) can also be written on a fluid of arbitrary depth, where it becomes

$$\eta_{tt} + \Omega^2 \eta + \epsilon N(\eta, \eta_t) = 0, \tag{2.5}$$

with

$$N(\eta, \eta_t) = \mathcal{L} \left(\frac{1}{2} (\nabla \mathcal{L}^{-1} \eta_t)^2 + \frac{1}{2}\eta_t^2 - \eta \Omega^2 \eta \right) - \nabla \cdot (\eta S \nabla \eta - \eta_t \nabla \mathcal{L}^{-1} \eta_t)$$

and

$$S = (1 - \sigma\Delta), \qquad \Omega^2 = S\mathcal{L}, \qquad \mathcal{L} = (-\Delta)^{1/2} \tanh((-\Delta)^{1/2} H_1).$$

In [15], (2.5) was derived to study deep-water gravity-capillary wave dynamics—the case $\sigma = 1$ with $H = \infty$. The above derivation makes no assumption on either H or σ, and thus it is natural to consider general Bond numbers and depths. In this work we will restrict our attention to the infinite-depth case, so further references to a weakly nonlinear model will be to (2.4).

3. Computing traveling waves. In this section we explain some of the novel computational considerations necessary for the numerical simulation of traveling wave solutions of the water wave problem (2.1). We also summarize the method used to compute solutions to the weakly nonlinear model (2.4). We begin with the former, an extension of the *Transformed Field Expansions* (TFE) approach of [14], and then proceed to the spectral collocation/Newton's method utilized for the latter.

Before describing the TFE approach, we recall a crucially important domain decomposition which can be made for the water wave problem with the introduction of an "artificial boundary." The details of this are provided in [14], but we summarize here for completeness. Our goal is to replace (2.1b) with an equivalent condition in the near-field, so consider (2.1a) and (2.1b),

$$\begin{aligned} \Delta\phi + \phi_{zz} &= 0, \qquad -H_0 < z < \eta, \\ \phi_z &= 0, \qquad z = -H_0, \end{aligned}$$

and notice that, given a plane $\{z = -a\}$ $(-H_0 < -a < -\|\eta\|_\infty)$, these are equivalent to

$$\Delta\phi + \phi_{zz} = 0, \qquad -a < z < \eta, \tag{3.1a}$$

$$\phi_z = \mu_z, \qquad z = -a, \tag{3.1b}$$

$$\phi = \mu, \qquad z = -a, \tag{3.1c}$$

$$\Delta\mu + \mu_{zz} = 0, \qquad -H_0 < z < a, \tag{3.1d}$$

$$\mu_z = 0, \qquad z = -H_0. \tag{3.1e}$$

If we denote $\phi(x, y, -a)$ by the variable $\psi(x, y)$, then it is clear that (3.1c), (3.1d), and (3.1e) have the unique solution

$$\mu(x, y, z) = \sum_{\mathbf{k}} \hat{\psi}_{\mathbf{k}} \frac{\cosh(|\mathbf{k}|(z+h))}{\cosh(|\mathbf{k}|(h-a))} e^{i\mathbf{k}\cdot(x,y)},$$

where $\hat{\psi}_{\mathbf{k}}$ is the $\mathbf{k}$th Fourier coefficient of $\psi(x, y)$. To close (3.1a) and (3.1b) for ϕ alone we simply need to produce $\mu_z(x, y, -a)$, which is delivered by the operator T,

$$T[\psi(x)] := \sum_{\mathbf{k}} |\mathbf{k}| \tanh\left((h-a)|\mathbf{k}|\right) \hat{\psi}_{\mathbf{k}} e^{i\mathbf{k}\cdot(x,y)},$$

a Fourier multiplier of order one. Thus, (3.1b) equivalently reads

$$\phi_z(x, y, -a) - T\phi(x, y, -a) = 0,$$

and we note that the infinite-depth case can be handled seamlessly with the observation that, when $h = \infty$,

$$T[\psi(x)] := \sum_{\mathbf{k}} |\mathbf{k}| \hat{\psi}_{\mathbf{k}} e^{i\mathbf{k}\cdot(x,y)}.$$

With this operator (2.1) can be *equivalently* restated on the truncated (and finite) domain $\{-a < z < \eta\}$, as

$$\Delta\phi + \phi_{zz} = 0, \qquad -a < z < \eta, \tag{3.2a}$$

$$\phi_z - T\phi = 0, \qquad z = -a, \tag{3.2b}$$

$$\eta_t + \nabla\eta \cdot \nabla\phi = \phi_z, \qquad z = \eta, \tag{3.2c}$$

$$\phi_t + \frac{1}{2}|\nabla\phi|^2 + \frac{1}{2}(\phi_z)^2 + g\eta - \gamma\nabla \cdot \left(\frac{\nabla\eta}{(1+|\nabla\eta|^2)^{1/2}}\right) = 0, \qquad z = \eta. \tag{3.2d}$$

To search for traveling waves we move to a reference frame moving uniformly with velocity $c \in \mathbb{R}^2$ and seek steady solutions. This results in the system of equations

$$\Delta\phi + \phi_{zz} = 0, \qquad -a < z < \eta, \tag{3.3a}$$

$$\phi_z - T\phi = 0, \qquad z = -a, \tag{3.3b}$$

$$c \cdot \nabla\eta + \nabla\eta \cdot \nabla\phi = \phi_z, \qquad z = \eta, \tag{3.3c}$$

$$c \cdot \nabla\phi + \frac{1}{2}|\nabla\phi|^2 + \frac{1}{2}(\phi_z)^2 + g\eta - \gamma\nabla \cdot \left(\frac{\nabla\eta}{(1+|\nabla\eta|^2)^{1/2}}\right) = 0, \qquad z = \eta. \tag{3.3d}$$

To summarize the TFE approach for computing traveling water waves, we begin with the domain-flattening change of variables

$$x' = x, \quad y' = y, \quad z' = a\left(\frac{z-\eta}{a+\eta}\right),$$

which are known as σ-coordinates [36] in atmospheric science and the C-method [37] in the electromagnetic theory of gratings. Defining the transformed potential

$$u(x', y', z') := \phi\left(x', y', \frac{(a+\eta)z'}{a} + \eta\right),$$

(3.3) becomes, upon dropping primes,

$$\Delta u + u_{zz} = F(x,y,z;u,\eta), \qquad -a < z < 0, \tag{3.4a}$$

$$u_z - Tu = J(x,y;u,\eta), \qquad z = -a, \tag{3.4b}$$

$$c\cdot\nabla\eta - u_z = Q(x,y;u,\eta,c), \qquad z = 0, \tag{3.4c}$$

$$c\cdot\nabla u + g\eta - \gamma\Delta\eta = R(x,y;u,\eta,c), \qquad z = 0, \tag{3.4d}$$

where the precise forms for F, J, Q, and R are reported in [14]. For the purposes of our brief explanation, the only salient feature of these inhomogeneities is that if $\eta = O(\delta)$ and $u = O(\delta)$, then they are $O(\delta^2)$. The TFE approach now posits the expansions

$$c = c(\delta) = c_0 + \sum_{n=1}^{\infty} c_n\delta^n, \quad \eta = \eta(x,y;\delta) = \sum_{n=1}^{\infty}\eta_n(x,y)\delta^n,$$

$$u = u(x,y,z;\delta) = \sum_{n=1}^{\infty} u_n(x,y,z)\delta^n, \tag{3.5}$$

which, a posteriori, can be shown to be *strongly* convergent [38]. Inserting these forms into (3.4) yields

$$\Delta u_n + u_{n,zz} = F_n(x,y,z), \qquad -a < z < 0, \tag{3.6a}$$

$$u_{n,z} - Tu_n = J_n(x,y), \qquad z = -a, \tag{3.6b}$$

$$c_0\cdot\nabla\eta_n - u_{n,z} = Q_n(x,y) - c_{n-1}\cdot\nabla\eta_1, \qquad z = 0, \tag{3.6c}$$

$$c_0\cdot\nabla u_n + g\eta_n - \gamma\Delta\eta_n = R_n(x,y) - c_{n-1}\cdot\nabla u_1, \qquad z = 0. \tag{3.6d}$$

Again, the forms for F_n, J_n, Q_n, and R_n can be found in [14] save for the contribution of the curvature term (which reflects the force due to surface tension) in R_n, which we now detail below. It is the incorporation of this term into our algorithm which is the computational novelty of this work.

To begin, let us define the curvature term

$$H(\nabla\eta) := \nabla\cdot\left[\frac{\nabla\eta}{(1+|\nabla\eta|^2)^{1/2}}\right]$$

and notice that

$$H(\nabla\eta) = \nabla\cdot\left[(\nabla\eta)F(\nabla\eta)\right],$$

where

$$F(\nabla\eta) := \frac{1}{(1+(\nabla\eta)\cdot(\nabla\eta))^{1/2}}.$$

When applied to η, (3.5), this can be written as

$$F(x,y;\delta) = \sum_{n=0}^{\infty} F_n(x,y)\delta^n,$$

from which we can easily find H_n:

$$H_n(x,y) = \nabla\cdot\left[\sum_{l=1}^{n}(\nabla\eta_l)F_{n-l}\right].$$

It is now crucially important to find a good formula for F_n, and for this we use the identity

$$F^2 = \frac{1}{1+\eta_x^2+\eta_y^2},$$

which implies that

$$F^2 + \eta_x^2 F^2 + \eta_y^2 F^2 = 1.$$

Expanding in Taylor series, we obtain

$$\left(\sum_{n=0}^{\infty} F_n \delta^n\right)^2 + \left(\sum_{n=1}^{\infty} \eta_{n,x}\delta^n\right)^2 \left(\sum_{n=0}^{\infty} F_n \delta^n\right)^2 + \left(\sum_{n=1}^{\infty} \eta_{n,y}\delta^n\right)^2 \left(\sum_{n=0}^{\infty} F_n \delta^n\right)^2 = 1,$$

which gives

$$\sum_{n=0}^{\infty}\left(\sum_{l=0}^{n} F_{n-l}F_l\right)\delta^n + \left[\sum_{n=2}^{\infty}\left(\sum_{l=1}^{n-1}\eta_{n-l,x}\eta_{l,x}\right)\delta^n\right]\left[\sum_{n=0}^{\infty}\left(\sum_{l=0}^{n} F_{n-l}F_l\right)\delta^n\right] + \left[\sum_{n=2}^{\infty}\left(\sum_{l=1}^{n-1}\eta_{n-l,y}\eta_{l,y}\right)\delta^n\right]\left[\sum_{n=0}^{\infty}\left(\sum_{l=0}^{n} F_{n-l}F_l\right)\delta^n\right] = 1.$$

At order zero it is not difficult to show that $F_0 = 1$. For $n \geq 1$ we have

$$2F_0F_n = -\sum_{l=1}^{n-1} F_{n-l}F_l - \sum_{m=0}^{n-2}\left(\sum_{q=1}^{n-m-1}\eta_{n-m-q,x}\eta_{q,x}\right)\left(\sum_{l=0}^{m} F_{m-l}F_l\right) - \sum_{m=0}^{n-2}\left(\sum_{q=1}^{n-m-1}\eta_{n-m-q,y}\eta_{q,y}\right)\left(\sum_{l=0}^{m} F_{m-l}F_l\right),$$

which, using $F_0 = 1$, gives

$$F_n = -\frac{1}{2}\sum_{l=1}^{n-1} F_{n-l}F_l - \frac{1}{2}\sum_{m=0}^{n-2}\sum_{q=1}^{n-m-1}\sum_{l=0}^{m}\eta_{n-m-q,x}\eta_{q,x}F_{m-l}F_l - \frac{1}{2}\sum_{m=0}^{n-2}\sum_{q=1}^{n-m-1}\sum_{l=0}^{m}\eta_{n-m-q,y}\eta_{q,y}F_{m-l}F_l.$$

With these formulas in hand for F_n, and thus H_n, we proceed as outlined in [14] with a Fourier-collocation/Chebyshev-tau approximation (with $N_1 \times N_2$ Fourier modes and $N_y + 1$ Chebyshev coefficients) of the problem (3.6) at every perturbation order $0 \leq n \leq N$. These partial Taylor sums can then be summed either directly or with the assistance of Padé approximation.

The numerical method used to compute solutions to (2.4) is a combination of spectral collocation and Newton's method. Traveling solutions are expanded in Fourier components,

$$\eta(x,t) \approx \eta_M(x,t) := \sum_{n=-M/2}^{M/2} a_n e^{ik_n(x-ct)}.$$

We take $a_0 = 0$, as the mean level has no meaning for a fluid of infinite depth. This transforms (2.4) into a nonlinear system of M algebraic equations for $M+1$ unknowns: the remaining M Fourier amplitudes and the speed c. To close the system we add an equation fixing $||\eta||_\infty$. Newton's method is used to find solutions to this system, with the linear solution as an initial guess. Solutions for different amplitudes are computed by continuation, as in [39, 40].

4. Results. In this section we present the numerical results—both some computed sample profiles and the speed-amplitude curves of solution branches. We begin by presenting some computed profiles. Next, we present the first three terms in a Stokes-like asymptotic expansion for each model. We then compare the low-order Stokes prediction to the numerical results in each model.

In Figure 4.1 we display sample profiles (the solutions featuring circles) of deep-water waves for two values of the surface tension σ and two values of the perturbation parameter δ. The nonlinear contributions are particularly evident in the case $\sigma = 0.34$ with the flattened trough and peaked crest. We include comparisons of waves moving at the same speed, where the two profiles differ in amplitude, as well as two profiles with matching amplitude, where the waves move at slightly different speeds. This

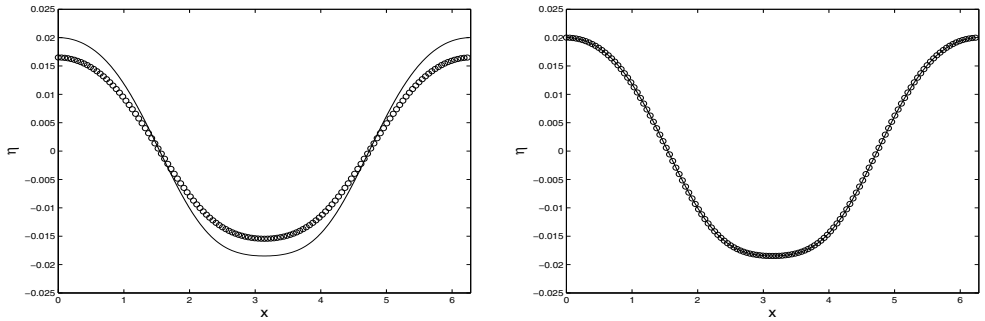

(a) $\sigma = 0.34$ (b) $\sigma = 0.34$

(c) $\sigma = 1$ (d) $\sigma = 1$

FIG. 4.1. *Profiles of computed traveling wave solutions to* (2.4) *(solid lines) are compared to those of* (2.2) *(circles). In the left column profiles are compared which move at the same speed, and in the right column with the same amplitude. In panel* 4.1(a) *the wave travels at speed* $c = 1.15791$*; in panel* 4.1(b) *the amplitude* $||\eta||_\infty = 0.02$*; in panel* 4.1(c) *the speed* $c = 1.41407$*; in panel* 4.1(d) *the amplitude* $||\eta||_\infty = 0.02$.

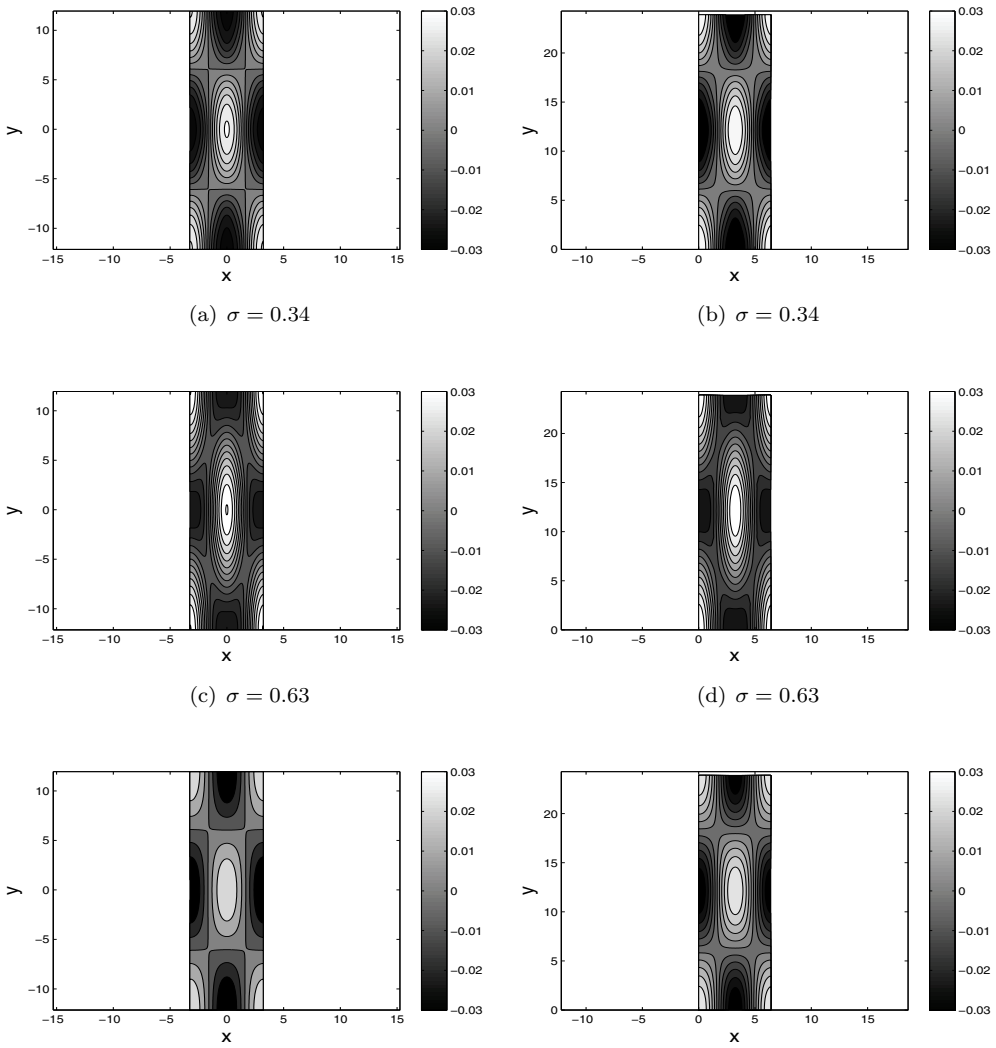

(a) $\sigma = 0.34$ (b) $\sigma = 0.34$

(c) $\sigma = 0.63$ (d) $\sigma = 0.63$

(e) $\sigma = 1$ (f) $\sigma = 1$

FIG. 4.2. *Contours of the free-surface displacement of three-dimensional traveling waves in* (2.4)*, left, and in the potential flow equations* (2.2)*, right. The waves are chosen to have* $||\eta||_\infty = 0.03$*, wave vectors angled from the propagation direction at* $\theta = \pi/12$*, and (from top to bottom) with Bond numbers* $\sigma = 0.34$*,* 0.63*, and* 1*. Observe that waves in the weakly nonlinear model,* (2.4)*, are qualitatively similar to those in potential flow, even near resonances. The locations of these waves relative to resonant waves can be seen in Figure* 4.5*.*

comparison illustrates that the error of (2.4) in approximating (2.2) can be thought of as either in amplitude *or* speed. Waves of the same small amplitude have virtually identical profiles but move at different speeds (see the right column in Figure 4.1). In Figure 4.2 (right column) contour plots are presented of two-dimensional surfaces (on a three-dimensional ocean) of deep-water short-crested waves. These are for three different values of the surface tension σ, and the nonlinear effects here are most evident near a Wilton ripple at $\sigma = 0.63$ (marked by a star in the left panel of Figure 4.5).

In addition to computing profiles, we compare branches of numerically computed traveling waves of both the potential flow equations (2.2) and the weakly nonlinear model (2.4) to the respective small amplitude predictions of low-order Stokes expansions. We use speed-amplitude plots as a basis for comparison. The computation of the terms in the Stokes expansion is a classic technique; see [3, 4, 5, 6, 7, 8]. The asymptotic approximations are used, in tandem with numerical solutions, to draw conclusions about the validity of the weakly nonlinear model (2.4) as an approximation of the potential flow equations. The asymptotic solutions are calculated with a classical Stokes expansion,

$$\eta = \epsilon\eta_1 + \epsilon^2\eta_2 + \epsilon^3\eta_3 + \cdots, \tag{4.1a}$$

$$\Phi = \epsilon\Phi_1 + \epsilon^2\Phi_2 + \epsilon^3\Phi_3 + \cdots, \tag{4.1b}$$

$$c = c_0 + \epsilon c_1 + \epsilon^2 c_2 + \cdots, \tag{4.1c}$$

though, due to the form of (2.4), the expansion of Φ is unnecessary. For a two-dimensional fluid, the leading order solution solves the linear problem (identical in both equations)

$$\eta_1 = e^{ix} + * = 2\cos(x), \tag{4.2a}$$

$$c_0 = \sqrt{1+\sigma}. \tag{4.2b}$$

Here and throughout, $*$ refers to the complex conjugate. The speed c_0 is the phase speed of a linear solution, $c_p = \frac{\omega}{k} = \sqrt{\frac{1}{|k|} + \sigma|k|}$, evaluated at $k = 1$. At second order, (2.4) also agrees with (2.2), both have $c_1 = 0$, and

$$\eta_2 = \frac{1+\sigma}{1-2\sigma}e^{2ix} + * = \frac{2+2\sigma}{1-2\sigma}\cos(2x).$$

We point out that the coefficient of the second harmonic, $\frac{2+2\sigma}{1-2\sigma}$, changes sign at $\sigma = 1/2$, and the sign of this correction corresponds to the well-known flattening of the crests and sharpening of the troughs for capillary waves, which is the reverse of gravity waves. At the critical value $\sigma = 1/2$, the linear wave resonates with its harmonic. Although the Stokes expansion about a single wave is singular here, a perturbation expansion does exist about a wave with two frequencies, called a Wilton ripple [7, 9]. For $\sigma = 1/2$ the leading order solution is

$$\eta_1 = e^{ix} \pm \frac{1}{2}e^{2ix} + * \qquad \text{and} \qquad c_0 = \sqrt{3/2}. \tag{4.3}$$

The correction to the speed and the free surface are the same in both (2.4) and (2.2),

$$\eta_2 = \mp 3e^{3ix} - e^{4ix} + * \qquad \text{and} \qquad c_1 = \pm\sqrt{3/8}. \tag{4.4}$$

In the neighborhood of second-order resonances, solutions to the quadratic model (2.4) may be better approximation to solutions of (2.2) than a third-order Stokes expansion.

At third order, the Stokes wave corrections in (2.2) and (2.4) differ; for the weakly nonlinear equation (2.4), with an extra subscript W (for weakly), the corrections are

$$c_{2,W} = \frac{(1+\sigma)^{3/2}}{1-2\sigma}, \tag{4.5a}$$

$$\eta_{3,W} = \frac{2(1+\sigma)^2}{(1-3\sigma)(1-2\sigma)}e^{3ix} + * = \frac{4(1+\sigma)^2}{(1-3\sigma)(1-2\sigma)}\cos(3x). \tag{4.5b}$$

The correction $\eta_{3,W}$ is singular both at $\sigma = 1/2$ and $\sigma = 1/3$, as can be seen by the factors of $(1-2\sigma)$ and $(1-3\sigma)$ in the denominator of $\eta_{3,W}$. This singularity is an artifact of the first and second Wilton ripples—the mth correction will be singular at $\sigma = 1/2, 1/3, \ldots, 1/m$. For the potential flow equations (2.2), with an extra subscript P (for potential), the corrections are

$$c_{2,P} = \frac{\sqrt{1+\sigma}(2\sigma^2+\sigma+8)}{4(1-2\sigma)(1+\sigma)}, \tag{4.6a}$$

$$\eta_{3,P} = \frac{6\sigma^2+21\sigma+6}{4(1-2\sigma)(1-3\sigma)}e^{3ix} + * = \frac{6\sigma^2+21\sigma+6}{2(1-2\sigma)(1-3\sigma)}\cos(3x). \tag{4.6b}$$

The correction to the displacement in the potential flow equations $\eta_{3,P}$ is also singular, $\sigma = 1/2$ and $1/3$. Just as with the model (2.4), the correction $\eta_{n,P}$ will be singular at $\sigma = \frac{1}{m}$ for $m = 2$ to n. Although the values of the corrections $c_{2,P}$ and $\eta_{3,P}$ are different from $c_{2,W}$ and $\eta_{3,W}$, quick inspection reveals that they share the same sign and are of the same order of magnitude. This is of particular importance because of the second role c_2 plays: predicting the evolution of weakly nonlinear wavepackets in the nonlinear Schrödinger (NLS) equation. To derive NLS, consider the alternate ansatz for the free-surface displacement

$$\eta = \epsilon A(\epsilon(x-c_g t), \epsilon^2 t)e^{ik_0 x - i\omega(k_0)t} + \epsilon^2 A_2(x,t) + \epsilon^3 A_3(x,t) + *. \tag{4.7}$$

When (4.7) is substituted into (2.4), the leading order amplitude A solves the NLS equation

$$iA_\tau + \frac{\omega''(k_0)}{2}A_{XX} = c_2|A|^2 A,$$

with $\tau = \epsilon^2 t$ and $X = \epsilon(x - c_g t)$ (see [41]). The NLS coefficient $c_{2,W}$ has been computed for (2.4) with $\sigma = 1$ in [15]; the NLS coefficient $c_{2,P}$ has been computed for other forms of the potential flow equations with surface tension [42, 43, 44]. Because of the correspondence between the perturbation expansion and the NLS equation, some credit for the original derivation of the nonlinear coefficient of the NLS equation for potential flow with surface tension should go to [8], who first found the third-order terms in the Stokes expansion for potential flow with surface tension in arbitrary depths.

In this paper we consider steady features of (2.4) and (2.2)—traveling profiles and speed-amplitude relations. For the depths and Bond numbers where the steady calculations show good agreement, one might consider using (2.4) to approximate the dynamics of (2.2). The second correction c_2, in addition to correcting the speed, is predictive with respect to the dynamics of periodic waves. In the NLS equation, the relative signs of the linear term and the nonlinear term determine the qualitative nature of the dynamics. The sign of c_2 predicts focusing or scattering of compactly supported data in the NLS equation, and predicts the stability of plane waves in the model equation (the Benjamin–Feir instability [45]). Because these are qualitative features, it is critical that the truncated equation (2.4) agrees with the potential flow equations (2.2) in terms of the relative signs of ω'' and c_2. Should the signs in one equation differ from the signs in the other, the qualitative *dynamics* will not be similar regardless of how small a wave is considered. Thus we note that (2.4) should not be used to approximate dynamics of (2.2) at Bond numbers where $c_{2,p}c_{2,w} < 0$. Brief examination reveals that $c_{2,p}c_{2,2} > 0$ for all σ in deep water on a two-dimensional fluid.

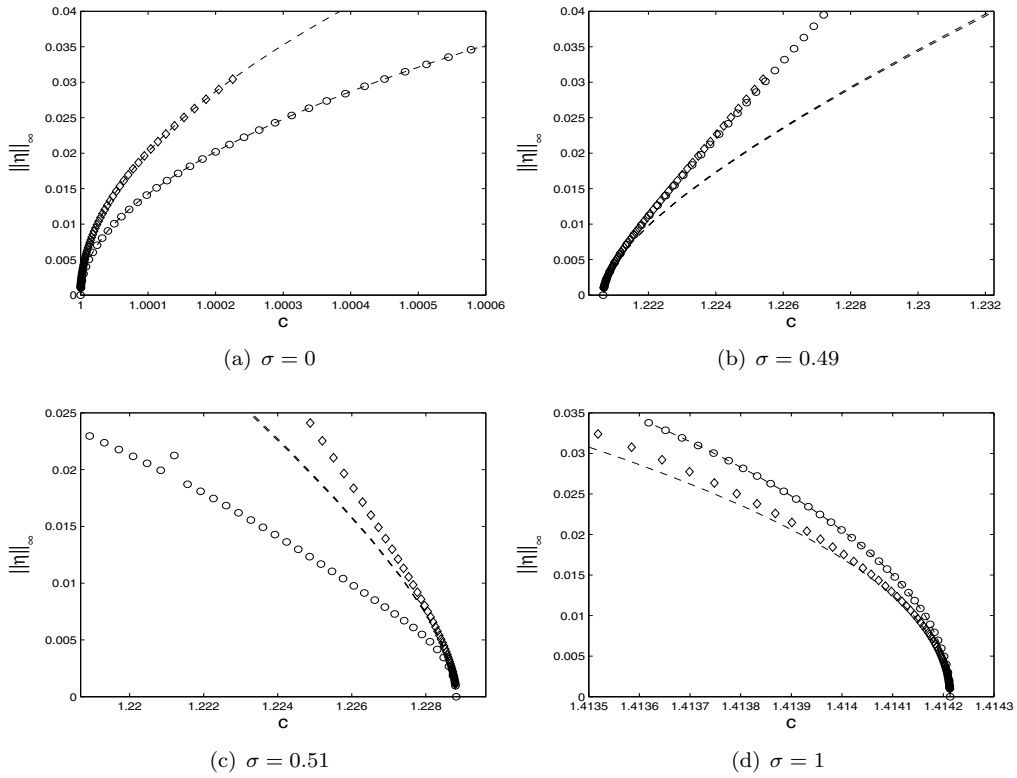

(a) $\sigma = 0$ (b) $\sigma = 0.49$

(c) $\sigma = 0.51$ (d) $\sigma = 1$

FIG. 4.3. *Numerically computed speed-amplitude curves for branches of two-dimensional traveling waves in the weakly nonlinear equation* (2.4) *(diamonds) compared to those in the potential flow equations* (2.2) *(circles), along with their third-order asymptotics (dashed lines). At* $\sigma = 0.49$*, near the Wilton ripple* $\sigma = 1/2$*, the weakly nonlinear model approximates the potential flow equations, but the asymptotic solution does not.*

The speed-amplitude curves of traveling waves on the surface of two-dimensional fluid—in both (2.2) and (2.4)—for a sample of Bond numbers, $\sigma = 0$, 0.49, 0.51, and 1, are plotted in Figure 4.3. The Bond numbers $\sigma = 1/2 \pm 0.01$ were chosen to observe waves near the first Wilton ripple $\sigma = 1/2$. The wave at $\sigma = 0$ is the limit point of the set of ripples $\sigma = 1/n$, where the resonance occurs at $O(\epsilon^n)$ as $n \to \infty$; no resonance actually occurs here. The Bond number $\sigma = 1$ corresponds to the capillary-gravity wavelength for which (2.4) was originally derived: no ripples occur near this Bond number. In Figure 4.3 one may observe the effects of resonances on the approximations of both the Stokes expansion and the weakly nonlinear model. Neither third-order Stokes expansion approximates the numerical solutions near $\sigma = 1/2$ very well. The weakly nonlinear model does appear to approximate the potential flow equations well at $\sigma = 0.49$, better than the third-order Stokes expansion. Away from resonances, both the weakly nonlinear model and the potential flow equations are well approximated by their respective third-order Stokes expansions.

For periodic waves on the surface of a three-dimensional fluid, we assume that the leading order solutions include two wavevectors at an angle, θ, to the propagation

direction,

$$\eta_1 = e^{i\mathbf{k_1}\cdot\mathbf{x}} + e^{i\mathbf{k_2}\cdot\mathbf{x}} + * = e^{i\left(\cos(\theta)x+\sin(\theta)y\right)} + e^{i\left(\cos(\theta)x-\sin(\theta)y\right)} + *, \tag{4.8a}$$

$$c_0 = \frac{\sqrt{1+\sigma}}{\cos(\theta)}, \tag{4.8b}$$

which are typically called short-crested waves [16]. We consider deep-water Stokes waves as a function of two free parameters, the Bond number σ and the angle θ. The corrections in the Stokes expansion about these waves are significantly more complicated, and for brevity are omitted.

On a two-dimensional fluid, resonant waves occur only at Bond numbers $\sigma = 1/n$ for integer n. On a three-dimensional fluid these resonances persist, and new resonances arise due to the additional geometric dependence of the leading order solution. The set of all resonant waves as functions of σ and θ satisfy the relation

$$\hat{\Omega}^2(m\mathbf{k_1} + n\mathbf{k_2}) - (m+n)^2(1+\sigma) = 0, \tag{4.9}$$

where

$$m, n \in \mathbb{Z}, \qquad \mathbf{k_j} = (\cos(\theta), (-1)^j \sin(\theta)), \qquad \hat{\Omega}^2(\mathbf{k}) = |\mathbf{k}|(1+\sigma|\mathbf{k}|^2).$$

A simple example of a resonance which depends on θ (with $m = n = 1$) appears in Figure 4.5 as a solid curve in the σ-θ plane. This resonance occurs at $O(\epsilon^2)$; more generally resonances appear at $O(\epsilon^{|n|+|m|})$. These resonances, although dependent on geometry, are generated by the same mechanism as the two-dimensional Wilton ripples, and we refer to them as such. An example of a Wilton ripple with geometric dependence is

$$\theta^* = \pi/12 \qquad \text{and} \qquad \sigma^* = \frac{2-\cos(\pi/12)}{4\cos^3(\pi/12)-2} \approx 0.644,$$

about which we have numerically simulated the near resonant waves at $(\theta, \sigma) = (\pi/12, 0.63)$ and $(\pi/12, 0.65)$. Near any resonance, perturbation expansions of the wave profile will not be valid. One may hope, however, that the quadratic model could capture the behavior of the full model near resonances which occur at quadratic order.

In Figure 4.4 we present the speed-amplitude curves for a selection of Bond numbers, $\sigma = 0$, 0.49, 0.51, 0.63, 0.65, and 1, which propagate at an angle $\theta = \pi/12$. The values $\sigma = 0.49$ and 0.51 bracket a quadratic resonance, as do the values $\sigma = 0.63$ and 0.65—these and other resonances are discussed at length in the following paragraph. We observe that near the the quadratic resonances ($\sigma = 0.49, 0.51, 0.63, 0.65$) the Stokes expansions do not well approximate numerical solutions of potential flow or the weakly nonlinear model. Away from the quadratic resonances ($\sigma = 0, 1$) both the weakly nonlinear model (2.4) and the potential flow equations are well approximated by their Stokes expansions. Interestingly, the weakly nonlinear model appears to approximate the potential flow equations as one approaches a resonance from the left (smaller bond numbers) $\sigma = 0.49$ and 0.63, but not from right (larger bond numbers) $\sigma = 0.51$ and 0.65. This asymmetry is an area of current investigation. To better study the resonant case, the TFE method is being extended to compute Wilton ripples.

We have computed the speed correction $c_2(\sigma, \theta)$ as a function of Bond number σ and angle from the propagation direction θ for both the potential flow equations

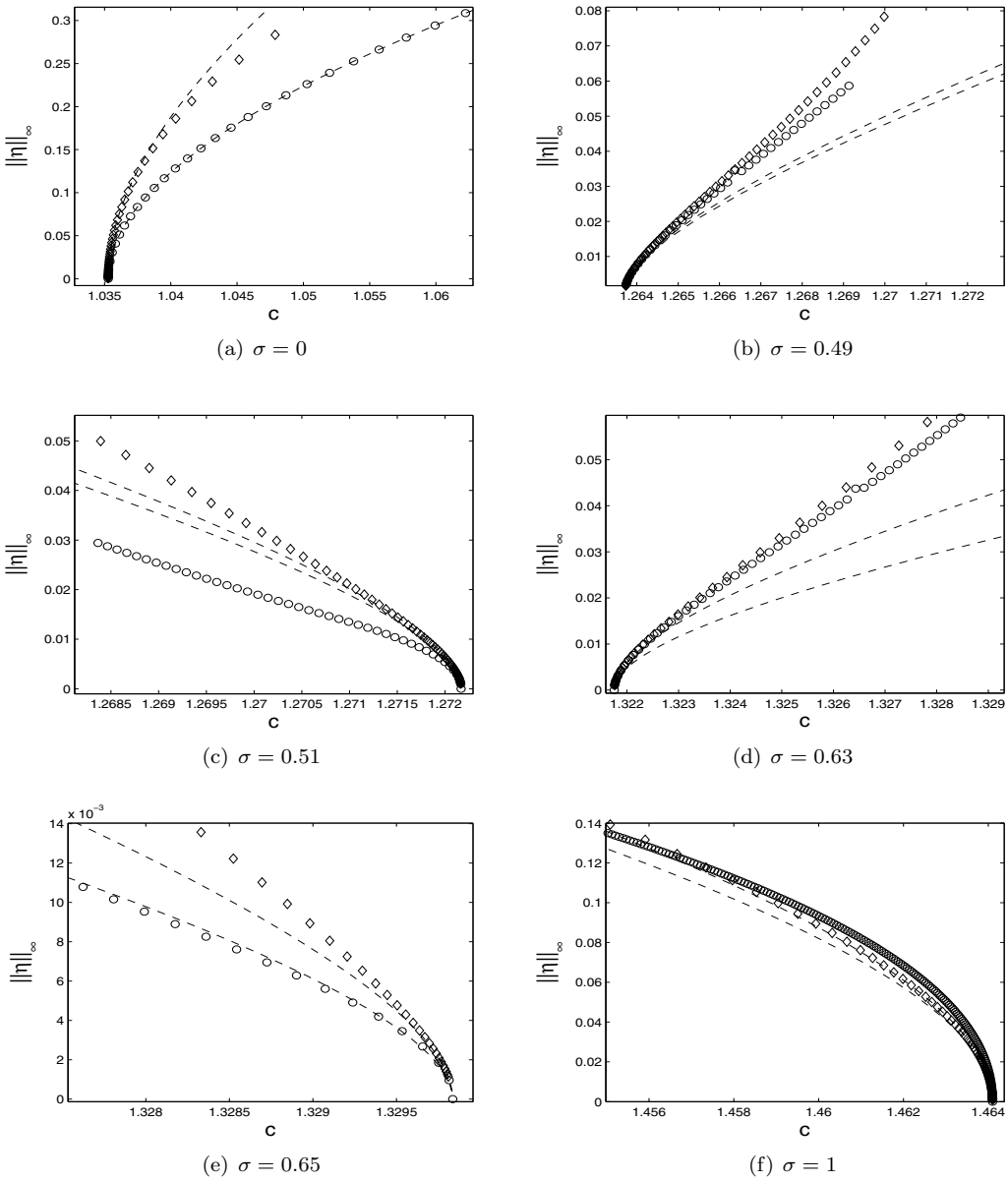

(a) $\sigma = 0$ (b) $\sigma = 0.49$

(c) $\sigma = 0.51$ (d) $\sigma = 0.63$

(e) $\sigma = 0.65$ (f) $\sigma = 1$

FIG. 4.4. *Numerically computed speed-amplitude curves for branches of three-dimensional traveling waves from the weakly nonlinear model* (2.4) *(diamonds) compared to those for potential flow* (2.2) *(circles), along with their third-order asymptotics (dashed lines). These waves are small perturbations of a linear wave with two wavenumbers which make angle of* $\theta = \pi/12$ *with the propagation direction.*

and the weakly nonlinear model. As mentioned for two-dimensional waves, the speed corrections c_2 depend on cubic interactions, some of which are neglected in the weakly nonlinear model equation (2.4); thus one should not expect $c_{2,W}$ to agree in value with $c_{2,P}$. We compare the signs of the corrections c_2 in Figure 4.5: in the light gray regions the sign of the $c_{2,W}$ does not agree with the sign of $c_{2,P}$. As discussed for

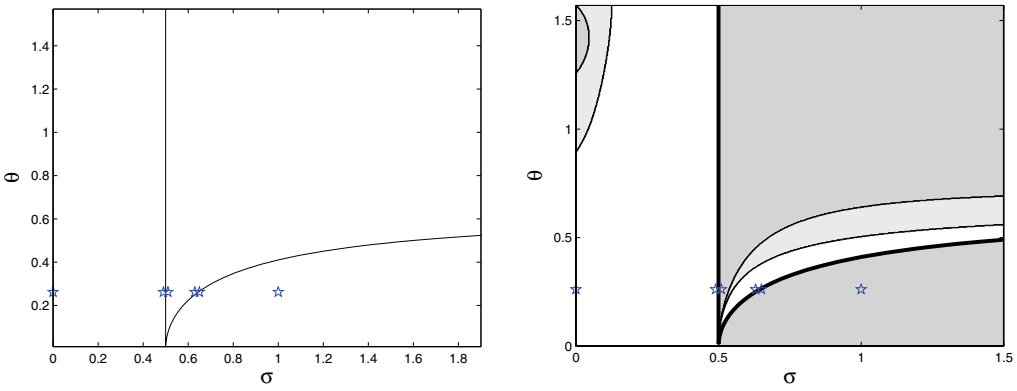

FIG. 4.5. *Left: The perturbation expansion for weakly nonlinear short-crested waves is singular on a countable set of curves in the σ-θ plane. The first of these curves, corresponding to $(m,n) = (0,2),(1,1)$ in (4.9), are marked with solid lines. The waves whose speed-amplitude curves are in Figure 4.4 are marked with stars. Right: The speed correction $c_2(\sigma,\theta)$ changes sign at the resonances $(m,n) = (0,2)$ and $(1,1)$—marked by the thick black curves in the right panel and the solid lines in the left panel. This correction also changes sign when there is some cancellation in the the nonlinearity, marked by the thinner curves in the right panel. Both speed corrections $c_{2,W}$ and $c_{2,P}$ are positive in the white region, while both are negative in the dark gray region. In the lighter gray region the signs differ with $c_{2,W} < 0$ and $c_{2,P} > 0$.*

a two-dimensional fluid, the sign of c_2 is predictive with respect to wave dynamics. Thus as an approximation of potential flow, (2.4) should be used only for *dynamics* of waves which are outside of the light gray regions in Figure 4.5. Equation (2.4) was originally derived to study waves near $(\sigma,\theta) = (1,0)$, which satisfy this criterion.

5. Conclusion. Periodic traveling wave solutions of the full water wave equations and a weakly nonlinear model for these on deep water are computed. Solutions to the weakly nonlinear model are computed by applying Newton's method to the truncated system of Fourier amplitudes. Solutions to the potential flow equations are computed using an extension of the method of Transformed Field Expansions [14].

The numerical solutions are compared to asymptotic predictions, made using a classic (Stokes) perturbation expansion. We compare the behavior of Stokes wave solutions to the potential flow equations to a quadratic truncation both apart from resonances and in the neighborhood of quadratic resonances. We observe that the quadratic model may approximate the potential flow equations better than the Stokes expansion near quadratic resonances. The performance of this approximation appears to be asymmetric about the resonant Bond numbers. To further investigate this asymmetry, the method of Transformed Field Expansions must be extended to compute Wilton ripples.

REFERENCES

[1] A. D. D. CRAIK, *The origins of water wave theory*, Ann. Rev. Fluid Mech., 36 (2004), pp. 1–28.

[2] A. D. D. CRAIK, *George Gabriel Stokes on water wave theory*, Ann. Rev. Fluid Mech., 37 (2005), pp. 23–42.

[3] W. J. HARRISON, *The influence of viscosity and capillarity on waves of finite amplitude*, Proc. Lond. Math. Soc., 7 (1909), pp. 107–121.

[4] R. J. C. Kamesvara, *On ripples of finite amplitude*, Proc. Indian Ass. Cultiv. Sci., 6 (1920), pp. 175–193.
[5] H. Lamb, *Hydrodynamics*, Cambridge University Press, Cambridge, UK, 1879.
[6] L. F. McGoldrick, *An experiment on second-order capillary gravity resonant wave interactions*, J. Fluid Mech., 40 (1970), pp. 251–271.
[7] J. Reeder and M. Shinbrot, *Three dimensional, nonlinear wave interaction in water of constant depth*, Nonlinear Anal., 5 (1981), pp. 303–323.
[8] W. J. Pierson and P. Fife, *Some nonlinear properties of long-crested periodic waves with lengths near* 2.44 *centimeters*, J. Geophys. Res., 66 (1961), pp. 163–179.
[9] J. R. Wilton, *On ripples*, Philos. Mag., 29 (1915), pp. 689–700.
[10] J.-M. Vanden-Broeck, *Wilton ripples generated by a moving pressure disturbance*, J. Fluid Mech., 451 (2002), pp. 193–201.
[11] J.-M. Vanden-Broeck, *Nonlinear gravity-capillary standing waves in water of arbitrary uniform depth*, J. Fluid Mech., 139 (1984), pp. 97–104.
[12] P. Christodoulides and F. Dias, *Resonant capillary-gravity interfacial waves*, J. Fluid Mech., 265 (1994), pp. 303–343.
[13] J. Reeder and M. Shinbrot, *On Wilton ripples* II: *Rigorous results*, Arch. Rational Mech. Anal., 77 (1981), pp. 321–347.
[14] D. P. Nicholls and F. Reitich, *Stable, high-order computation of traveling water waves in three dimensions*, Eur. J. Mech. B Fluids, 25 (2006), pp. 406–424.
[15] B. Akers and P. A. Milewski, *Dynamics of three-dimensional gravity-capillary solitary waves in deep water*, SIAM J. Appl. Math., 70 (2010), pp. 2390–2408.
[16] F. Dias and C. Kharif, *Nonlinear gravity and gravity-capillary waves*, Ann. Rev. Fluid Mech., 31 (1999), pp. 301–346.
[17] A. J. Roberts and L. W. Schwartz, *The calculation of nonlinear short-crested gravity waves*, Phys. Fluid, 26 (1983), pp. 2388–2392.
[18] D. P. Nicholls, *Traveling water waves: Spectral continuation methods with parallel implementation*, J. Comput. Phys., 143 (1998), pp. 224–240.
[19] L. W. Schwartz and J.-M. Vanden-Broeck, *Numerical solution of the exact equations for capillary-gravity waves*, J. Fluid Mech., 95 (1979), pp. 119–139.
[20] O. Kimmoun, H. Branger, and C. Kharif, *On short-crested waves: Experimental and analytical investigations*, Eur. J. Mech. B Fluids, 18 (1999), pp. 889–930.
[21] J. L. Hammack and D. M. Henderson, *Experiments on deep-water waves with two dimensional surface patterns*, J. Offshore Mech. Arct. Eng., 125 (2003), pp. 48–53.
[22] P. G. Saffman, *The superharmonic instability of finite amplitude water waves*, J. Fluid Mech., 159 (1985), pp. 169–174.
[23] T. R. Akylas and Y. Cho, *On the stability of lumps and wave collapse in water waves*, Philos. Trans. R. Soc. Lond. Ser. A Math. Phys. Eng. Sci., 366 (2008), pp. 2761–2774.
[24] B. Akers and P. A. Milewski, *A stability result for travelling waves in dispersive nonlinear equations*, Comm. Math. Sci., 6 (2008), pp. 791–797.
[25] A. D. D. Craik, *Wave Interactions and Fluid Flows*, Cambridge University Press, Cambridge, UK, 1985.
[26] D. P. Nicholls, *Boundary perturbation methods for water waves*, GAMM-Mitt., 30 (2007), pp. 44–74.
[27] A. J. Roberts, *Highly nonlinear short-crested water waves*, J. Fluid Mech., 135 (1983), pp. 301–321.
[28] T. R. Marchant and A. J. Roberts, *Properties of short-crested waves in water of finite depth*, J. Austral. Math. Soc. Ser. B, 29 (1987), pp. 103–125.
[29] D. P. Nicholls and J. Shen, *A rigorous numerical analysis of the transformed field expansion method*, SIAM J. Numer. Anal., 47 (2009), pp. 2708–2734.
[30] D. J. Korteweg and G. de Vries, *On the change in form of long waves advancing in a rectangular canal and new type of long stationary waves*, Philos. Mag., 39 (1895), pp. 422–443.
[31] B. B. Kadomtsev and V. I. Petviashvili, *On the stability of solitary waves in weakly dispersing media*, Soviet. Phys. Dokl., 15 (1970), pp. 539–541.
[32] D. R. Fuhrman and P. A. Madsen, *Short-crested waves in deep water: A numerical investigation of recent laboratory experiments*, J. Fluid Mech., 559 (2006), pp. 391–411.
[33] B. Akers and P. A. Milewski, *Model equations for gravity-capillary waves in deep water*, Stud. Appl. Math., 121 (2008), pp. 49–69.
[34] B. Akers and P. A. Milewski, *A model equation for wavepacket solitary waves arising from capillary-gravity flows*, Stud. Appl. Math., 122 (2009), pp. 249–274.
[35] N. B. Vargraftik, B. N. Volkov, and L. D. Voljak, *International tables of the surface tension of water*, J. Phys. Chem. Ref. Data, 12 (1983), pp. 817–820.

[36] N. A. Phillips, *A coordinate system having some special advantages for numerical forecasting*, J. Atmos. Sci., 14 (1957), pp. 184–185.
[37] J. Chandezon, D. Maystre, and G. Raoult, *A new theoretical method for diffraction gratings and its numerical application*, J. Opt., 11 (1980), pp. 235–241.
[38] D. P. Nicholls and F. Reitich, *On analyticity of traveling water waves*, Proc. R. Soc. Lond. Ser. A Math. Phys. Eng. Sci., 461 (2005), pp. 1283–1309.
[39] P. A. Milewski, *Three-dimensional localized gravity-capillary waves*, Comm. Math. Sci., 3 (2005), pp. 89–99.
[40] J.-M. Vanden-Broeck and F. Dias, *Gravity-capillary solitary waves in water of infinite depth and related free surface flows*, J. Fluid Mech., 240 (1992), pp. 549–557.
[41] M. J. Ablowitz and H. Segur, *On the evolution of packets of water waves*, J. Fluid Mech., 92 (1979), pp. 691–715.
[42] V. D. Djordjevic and L. G. Redekopp, *On two dimensional packets of capillary-gravity waves*, J. Fluid Mech., 79 (1977), pp. 703–714.
[43] T. Kawahara, *Nonlinear self-modulation of capillary-gravity waves on a liquid layer*, J. Phys. Soc. Japan, 38 (1975), pp. 265–270.
[44] T. R. Akylas, *Envelope solitons with stationary crests*, Phys. Fluids A, 5 (1993), pp. 789–791.
[45] T. B. Benjamin and J. E. Feir, *The disintegration of wave trains on deep water*, J. Fluid Mech., 27 (1967), pp. 417–430.